Front. Phys., 2013, 8(1): 20–26
DOI 10.1007/s11467-013-0284-1

RESEARCH ARTICLE

Demonstration of eight-partite two-diamond shape cluster state for continuous variables

Xiao-Long Su, Shu-Hong Hao, Ya-Ping Zhao, Xiao-Wei Deng, Xiao-Jun Jia, Chang-De Xie†, Kun-Chi Peng

State Key Laboratory of Quantum Optics and Quantum Optics Devices, Institute of Opto-Electronics, Shanxi University, Taiyuan 030006, China

E-mail: †changde@sxu.edu.cn

Received January 2, 2013; accepted January 10, 2013

Multipartite entangled state is the basic resource for implementing quantum information networks and quantum computation. In this paper, we present the experimental demonstration of the eight-partite two-diamond shape cluster states for continuous variables, which consist of eight spatially separated and entangled optical modes. Eight resource squeezed states of light with classical coherence are produced by four nondegenerate optical parametric amplifiers and then they are transformed to the eight-partite two-diamond shape cluster states by a specially designed linear optical network. Since the spatially separated multipartite entangled state can be prepared off-line, it can be conveniently applied in the future quantum technology.

Keywords quantum computation, continuous variable, cluster state, squeezed state

PACS numbers 03.67.Bg, 03.67.Lx, 03.65.Ud, 42.50.Dv

1 Introduction

Quantum information (QI) science has exhibited unusual potentiality in recent years [1, 2]. Optical QI exploiting discrete-variable (DV) of single-photon states (photonic qubits) and continuous-variable (CV) of optical modes (photonic qumodes) play important role for the development of QI in both fundamental research and application exploration. The one-way quantum computation (QC) based on multipartite cluster entanglement is initially proposed by Raussendorf and Briegel in the DV model [3], then it is extended to the CV regime by Menicucci *et al.* [4]. For one-way QC model the qubits (qumodes) are initialized in a multipartite cluster entangled state firstly, then a variety of quantum logical operations can be achieved only via the single-qubit (qumode) projective measurement and the classical feedforward of the measured outcomes, in which the order and choices of measurements are determined by the required algorithm [3]. The basic logical operations of one-way DVQC has been experimentally demonstrated by several groups [5–7].

Parallelly, the theoretical and experimental explorations on one-way CVQC have also been proceeding continually [8–14]. In contrast to the probabilistic generation of photonic qubits in most cases, CV cluster states are produced in an unconditional fashion and thus the one-way QC with CV cluster entangled photonic qumodes can be implemented deterministically [11–18]. Following the theoretical proposals on one-way CVQC the principally experimental demonstrations of various one-way QC logical operations over CVs were achieved by utilizing bipartite or four-partite cluster entangled photonic qumodes [11–14]. To develop more complicated QC larger cluster states with more numbers of entangled qubits (qumodes) are desired. Very recently, we experimentally prepared CV eight-partite linear cluster state with a one-dimensional structure [19]. In this paper, we present the first experimental achievement on producing CV eight-partite two-diamond shape entangled state, which has a two dimensional structure and thus has potential applications in complex CVQI network and CVQC. We use eight squeezed states of light to be the initial resource quantum states and pass through the linearly optical transformation on a specially designed beam-splitter network, the eight-partite two-diamond shape cluster states for photonic qumodes are prepared. The entanglement feature among the obtained

eight space-separated photonic qumodes is confirmed by the fully inseparability criteria for CV multipartite entangled states proposed by van Loock and Furusawa [20].

2 Preparation scheme of the cluster state

At first, we briefly introduce the definition of CV cluster state. The cluster state is a type of multipartite quantum entangled graph states corresponding to some mathematic graphs [4,10,21]. The CV cluster quadrature correlations (so-called nullifiers) are expressed by [10,21,22]

$$(\hat{p}_a - \sum_{b\in N_a} \hat{x}_b) \to 0, \quad \forall\, a \in G \tag{1}$$

where $\hat{x}_a = (\hat{a} + \hat{a}^\dagger)/2$ and $\hat{p}_a = (\hat{a} - \hat{a}^\dagger)/(2\mathrm{i})$ stand for the quadrature-amplitude and the quadrature-phase operators of an optical mode $\hat{a}$, respectively. The subscript a (b) expresses the designated mode $\hat{a}$ ($\hat{b}$). The modes of $a \in G$ denote the vertices of the graph G, while the modes of $b \in N_a$ are the nearest neighbors of mode $\hat{a}$. For an ideal cluster state the left-hand side of Eq. (1) trends to zero, which stands for a simultaneous zero eigenstate of the quadrature combination [10]. The CV cluster quantum entanglement generated by experiments is deterministic, but also is imperfect, the entanglement features of which have to be verified and quantified by the sufficient conditions for the fully inseparability of multipartite CV entanglement [15–18]. There are different correlation combinations [left-hand side of Eq. (1)] in a variety of CV cluster multipartite entangled states, which reflect the complexity and rich usability of these quantum systems. The expressions of the nullifiers for different graph states depend on their graph configurations.

Figure 1(a) shows the graph representations of CV eight-partite two-diamond shape cluster state, each node of which corresponds to an optical mode and the connection lines between neighboring nodes stand for the interaction between the nodes. From Eq. (1) and Fig. 1(a), we obtain the nullifiers of the two-diamond shape CV cluster state, which are $\hat{p}_{D_1} - \hat{x}_{D_3} - \hat{x}_{D_4} = \delta_{D_1}$, $\hat{p}_{D_2} - \hat{x}_{D_3} - \hat{x}_{D_4} = \delta_{D_2}$, $\hat{p}_{D_3} - \hat{x}_{D_1} - \hat{x}_{D_2} = \delta_{D_3}$, $\hat{p}_{D_4} - \hat{x}_{D_1} - \hat{x}_{D_2} - \hat{x}_{D_5} = \delta_{D_4}$, $\hat{p}_{D_5} - \hat{x}_{D_4} - \hat{x}_{D_7} - \hat{x}_{D_8} = \delta_{D_5}$, $\hat{p}_{D_6} - \hat{x}_{D_7} - \hat{x}_{D_8} = \delta_{D_6}$, $\hat{p}_{D_7} - \hat{x}_{D_5} - \hat{x}_{D_6} = \delta_{D_7}$, $\hat{p}_{D_8} - \hat{x}_{D_5} - \hat{x}_{D_6} = \delta_{D_8}$, where the subscripts D_i $(i = 1, 2, \cdots, 8)$ denote the individual nodes of the two-diamond shape cluster state, and δ_{D_i} express the excess noises resulting from the imperfect quantum correlations. When the variance of δ_{D_i} is smaller than the corresponding quantum noise limit (QNL) determined by vacuum noises, the correlations among the combined optical modes is within the quantum region, otherwise the quantum correlations do not exist.

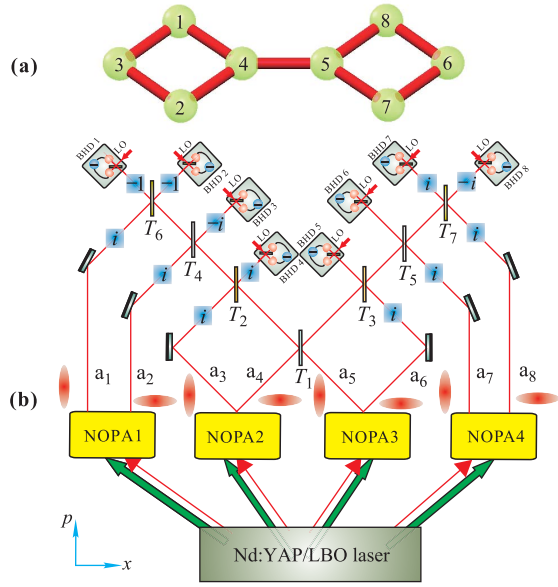

Fig. 1 **(a)** The graph representation of the two-diamond shape eight-partite cluster states. Each node corresponds to an optical mode. The connected lines between neighboring nodes stand for the interaction among these nodes. **(b)** Schematic of experimental setup for CV eight-partite two-diamond shape cluster state generation. T: Transmission efficient of beam splitter, Boxes including i express Fourier transforms (90° rotations in phase space), $-i$ express a $-90°$ rotation, and -1 express a 180° rotation, NOPA: The nondegenerate optical parametric amplifier, BHD: Balanced homodyne detector, LO: Local oscillator.

2.1 Unitary matrix of the linear transformation

The schemes of generating CV multipartite entangled states commonly used in experiments are to achieve a linearly optical transformation of input squeezed states on a specific beam-splitter network [21, 22]. According to the proposal of Refs. [21] and [22], CV cluster states of photonic qumodes can be created via a general linear-optics transformation of $\hat{p}$-squeezed input modes $\hat{a}_l = \mathrm{e}^{+r}\hat{x}_l^{(0)} + \mathrm{i}\mathrm{e}^{-r}\hat{p}_l^{(0)}$, where $\hat{x}_j^{(0)}$ and $\hat{p}_j^{(0)}$ denote the quadrature-amplitude and the quadrature-phase operators of the corresponding vacuum field, respectively, r is the squeezing parameter to quantify the squeezing level, $r = 0$ and $r = +\infty$ correspond to the two cases of no squeezing and the ideally perfect squeezing, respectively. Assuming $\hat{a}_l$ and U_{kl} stand for the input squeezed states and the unitary matrix of a given beam-splitter network, respectively, the output optical modes after the transformation are given by $\hat{b}_k = \sum_l U_{kl}\hat{a}_l$, where the subscripts l and k express the designated input and output modes, respectively. The CV cluster states satisfy $I\mathrm{Im}[UB_{in}] - A\mathrm{Re}[UB_{in}] \to 0$ in the limit of infinite squeezing, where I is the identity matrix, $B_{in} = (\hat{a}_1, \hat{a}_2, \cdots, \hat{a}_n)^{\mathrm{T}}$ denotes the matrix of input states, A is the adjacency matrix [23]. So we have $I\mathrm{Im}U = A\mathrm{Re}U$,

and obtain the unitary matrix:

$$U = (I + \mathrm{i}A)\mathrm{Re}U \tag{2}$$

Based on the unitarity of matrix U, $UU^\dagger = I$, we have

$$\mathrm{Re}U(\mathrm{Re}U)^{\mathrm{T}} = (I + A^2)^{-1} \tag{3}$$

In this case, we can calculate ReU and U from the adjacency matrix A.

For n-partite cluster state, assuming

$$\mathrm{Re}U = \begin{pmatrix} \vec{\alpha}_1^{\mathrm{T}} \\ \vec{\alpha}_2^{\mathrm{T}} \\ \vdots \\ \vec{\alpha}_n^{\mathrm{T}} \end{pmatrix} \tag{4}$$

where $\vec{\alpha}_i^{\mathrm{T}} = (\alpha_{i1}, \alpha_{i2}, \cdots, \alpha_{in})$ is a real vector. According to Eq. (3), we have $\vec{\alpha}_i^{\mathrm{T}}\vec{\alpha}_j = (I + A^2)^{-1}_{ij}$ $(i, j = 1, \cdots, n)$, and the numbers of these equations are $n(n+1)/2$ according to the symmetry of matrix. Since there are n^2 unknown numbers in all these equations, we need $n(n-1)/2$ conditions to solve the equations. For simplicity and without losing generality, some unknown numbers in the equations are chosen to be 0 when we solve the equations.

Since the unitary matrix of the two-diamond shape eight-partite cluster state can be obtained directly from that of the linear cluster state. We calculate the matrix elements for the linear cluster state, firstly. For CV eight-partite linear cluster state [19], the adjacency matrix is written as

$$A = \begin{pmatrix} 0 & 1 & 0 & 0 & 0 & 0 & 0 & 0 \\ 1 & 0 & 1 & 0 & 0 & 0 & 0 & 0 \\ 0 & 1 & 0 & 1 & 0 & 0 & 0 & 0 \\ 0 & 0 & 1 & 0 & 1 & 0 & 0 & 0 \\ 0 & 0 & 0 & 1 & 0 & 1 & 0 & 0 \\ 0 & 0 & 0 & 0 & 1 & 0 & 1 & 0 \\ 0 & 0 & 0 & 0 & 0 & 1 & 0 & 1 \\ 0 & 0 & 0 & 0 & 0 & 0 & 1 & 0 \end{pmatrix} \tag{5}$$

we have

$$(I + A^2)^{-1} = \begin{pmatrix} \frac{21}{34} & 0 & \frac{-4}{17} & 0 & \frac{3}{34} & 0 & \frac{-1}{34} & 0 \\ 0 & \frac{13}{34} & 0 & \frac{-5}{34} & 0 & \frac{1}{17} & 0 & \frac{-1}{34} \\ \frac{-4}{17} & 0 & \frac{8}{17} & 0 & \frac{-3}{17} & 0 & \frac{1}{17} & 0 \\ 0 & \frac{-5}{34} & 0 & \frac{15}{34} & 0 & \frac{-3}{17} & 0 & \frac{3}{34} \\ \frac{3}{34} & 0 & \frac{-3}{17} & 0 & \frac{15}{34} & 0 & \frac{-5}{34} & 0 \\ 0 & \frac{1}{17} & 0 & \frac{-3}{17} & 0 & \frac{8}{17} & 0 & \frac{-4}{17} \\ \frac{-1}{34} & 0 & \frac{1}{17} & 0 & \frac{-5}{34} & 0 & \frac{13}{34} & 0 \\ 0 & \frac{-1}{34} & 0 & \frac{3}{34} & 0 & \frac{-4}{17} & 0 & \frac{21}{34} \end{pmatrix} \tag{6}$$

The matrix elements in Eq. (4) are obtained in the following way. Considering the symmetry, we start from the middle row, $\vec{\alpha}_4^{\mathrm{T}} = (\alpha_{41}, \alpha_{42}, \alpha_{43}, \alpha_{44}, \alpha_{45}, \alpha_{46}, \alpha_{47}, \alpha_{48})$. We apply seven initial conditions, $\alpha_{41} = \alpha_{42} = \alpha_{43} = \alpha_{44} = \alpha_{46} = \alpha_{47} = \alpha_{48} = 0$, then it becomes $\vec{\alpha}_4^{\mathrm{T}} = (\ 0\ \ 0\ \ 0\ \ 0\ \ \alpha_{45}\ \ 0\ \ 0\ \ 0\ )$. According to equations $\vec{\alpha}_4^{\mathrm{T}}\vec{\alpha}_4 = (I + A^2)^{-1}_{44} = \frac{15}{34}$, the first matrix elements in Eq. (4) $\alpha_{45} = -\sqrt{\frac{15}{34}}$ is obtained. Then applying six conditions, $\alpha_{51} = \alpha_{52} = \alpha_{53} = \alpha_{56} = \alpha_{57} = \alpha_{58} = 0$ on $\vec{\alpha}_5^{\mathrm{T}}$, we obtain $\vec{\alpha}_5^{T} = (\ 0\ \ 0\ \ 0\ \ \alpha_{54}\ \ \alpha_{55}\ \ 0\ \ 0\ \ 0\ )$. Using equations $\vec{\alpha}_5^{\mathrm{T}}\vec{\alpha}_5 = (I + A^2)^{-1}_{55} = \frac{15}{34}$ and $\alpha_5^{\mathrm{T}}\alpha_4 = (I + A^2)^{-1}_{54} = 0$, we obtain two matrix elements in Eq. (4) $\alpha_{55} = 0$, and $\alpha_{54} = -\sqrt{\frac{15}{34}}$. In the same way, other matrix elements in Eq. (4) can be calculated.

After all the matrix elements in Eq. (4) are obtained, the unitary matrix is given from Eq. (2). The unitary matrix of the eight-partite linear cluster state transformed from eight $\hat{p}$-squeezed states are expressed by

$$U_L^p = \begin{pmatrix} \frac{1}{\sqrt{2}} & \frac{\mathrm{i}}{\sqrt{3}} & \frac{1}{\sqrt{10}} & \frac{-\sqrt{3}}{\sqrt{170}} & \frac{\mathrm{i}\sqrt{5}}{\sqrt{102}} & 0 & 0 & 0 \\ \frac{\mathrm{i}}{\sqrt{2}} & \frac{1}{\sqrt{3}} & \frac{-\mathrm{i}}{\sqrt{10}} & \frac{\mathrm{i}\sqrt{3}}{\sqrt{170}} & \frac{\sqrt{5}}{\sqrt{102}} & 0 & 0 & 0 \\ 0 & \frac{\mathrm{i}}{\sqrt{3}} & \frac{-\sqrt{2}}{\sqrt{5}} & \frac{\sqrt{6}}{\sqrt{85}} & \frac{-\mathrm{i}\sqrt{10}}{\sqrt{51}} & 0 & 0 & 0 \\ 0 & 0 & \frac{-\mathrm{i}\sqrt{2}}{\sqrt{5}} & \frac{-\mathrm{i}3\sqrt{3}}{\sqrt{170}} & \frac{-\sqrt{15}}{\sqrt{34}} & 0 & 0 & 0 \\ 0 & 0 & 0 & \frac{-\sqrt{15}}{\sqrt{34}} & \frac{-\mathrm{i}3\sqrt{3}}{\sqrt{170}} & \frac{\mathrm{i}\sqrt{2}}{\sqrt{5}} & 0 & 0 \\ 0 & 0 & 0 & \frac{-\mathrm{i}\sqrt{10}}{\sqrt{51}} & \frac{\sqrt{6}}{\sqrt{85}} & \frac{\sqrt{2}}{\sqrt{5}} & \frac{\mathrm{i}}{\sqrt{3}} & 0 \\ 0 & 0 & 0 & \frac{\sqrt{5}}{\sqrt{102}} & \frac{\mathrm{i}\sqrt{3}}{\sqrt{170}} & \frac{\mathrm{i}}{\sqrt{10}} & \frac{1}{\sqrt{3}} & \frac{-\mathrm{i}}{\sqrt{2}} \\ 0 & 0 & 0 & \frac{\mathrm{i}\sqrt{5}}{\sqrt{102}} & \frac{-\sqrt{3}}{\sqrt{170}} & \frac{-1}{\sqrt{10}} & \frac{\mathrm{i}}{\sqrt{3}} & \frac{-1}{\sqrt{2}} \end{pmatrix} \tag{7}$$

In our experiment, four quadrature-amplitude $\hat{x}$-squeezed states, $\hat{a}_m = \mathrm{e}^{-r}\hat{x}_m^{(0)} + \mathrm{i}\mathrm{e}^{+r}\hat{p}_m^{(0)}$ $(m = 1, 3, 5, 7)$, and four quadrature-phase $\hat{p}$-squeezed states, $\hat{a}_n = \mathrm{e}^{+r}\hat{x}_n^{(0)} + \mathrm{i}\mathrm{e}^{-r}\hat{p}_n^{(0)}$ $(n = 2, 4, 6, 8)$, are used as the resource states. Applying Fourier transformation on modes $\hat{a}_1, \hat{a}_3, \hat{a}_5$ and $\hat{a}_7$, which corresponds to multiplying i on the values of columns 1, 3, 5 and 7 of the unitary matrix U_L^p, we obtain the unitary matrix of CV eight-partite linear cluster state for our experimental system, which is

$$U_L = \begin{pmatrix} \frac{\mathrm{i}}{\sqrt{2}} & \frac{\mathrm{i}}{\sqrt{3}} & \frac{\mathrm{i}}{\sqrt{10}} & \frac{\sqrt{3}}{\sqrt{170}} & \frac{\sqrt{5}}{\sqrt{102}} & 0 & 0 & 0 \\ \frac{-1}{\sqrt{2}} & \frac{1}{\sqrt{3}} & \frac{1}{\sqrt{10}} & \frac{-\mathrm{i}\sqrt{3}}{\sqrt{170}} & \frac{-\mathrm{i}\sqrt{5}}{\sqrt{102}} & 0 & 0 & 0 \\ 0 & \frac{\mathrm{i}}{\sqrt{3}} & \frac{-\mathrm{i}\sqrt{2}}{\sqrt{5}} & \frac{-\sqrt{6}}{\sqrt{85}} & \frac{-\sqrt{10}}{\sqrt{51}} & 0 & 0 & 0 \\ 0 & 0 & \frac{\sqrt{2}}{\sqrt{5}} & \frac{\mathrm{i}3\sqrt{3}}{\sqrt{170}} & \frac{\mathrm{i}\sqrt{15}}{\sqrt{34}} & 0 & 0 & 0 \\ 0 & 0 & 0 & \frac{\sqrt{15}}{\sqrt{34}} & \frac{-3\sqrt{3}}{\sqrt{170}} & \frac{\mathrm{i}\sqrt{2}}{\sqrt{5}} & 0 & 0 \\ 0 & 0 & 0 & \frac{\mathrm{i}\sqrt{10}}{\sqrt{51}} & \frac{-\mathrm{i}\sqrt{6}}{\sqrt{85}} & \frac{\sqrt{2}}{\sqrt{5}} & \frac{1}{\sqrt{3}} & 0 \\ 0 & 0 & 0 & \frac{-\sqrt{5}}{\sqrt{102}} & \frac{\sqrt{3}}{\sqrt{170}} & \frac{\mathrm{i}}{\sqrt{10}} & \frac{-\mathrm{i}}{\sqrt{3}} & \frac{-\mathrm{i}}{\sqrt{2}} \\ 0 & 0 & 0 & \frac{-\mathrm{i}\sqrt{5}}{\sqrt{102}} & \frac{\mathrm{i}\sqrt{3}}{\sqrt{170}} & \frac{-1}{\sqrt{10}} & \frac{1}{\sqrt{3}} & \frac{-1}{\sqrt{2}} \end{pmatrix} \tag{8}$$

Similarly, we deduce the unitary matrix of CV eight-partite two-diamond shape cluster state (U_D) and find that it equals to a unitary transformation $U_F = \mathrm{diag}\{-1,-\mathrm{i},\mathrm{i},1,1,\mathrm{i},-\mathrm{i},-1\}$ of the unitary matrix U_L, i.e. $U_D = U_F U_L$, so we have

$$U_D = \begin{pmatrix} \frac{-\mathrm{i}}{\sqrt{2}} & \frac{-\mathrm{i}}{\sqrt{3}} & \frac{-\mathrm{i}}{\sqrt{10}} & \frac{-\sqrt{3}}{\sqrt{170}} & \frac{-\sqrt{5}}{\sqrt{102}} & 0 & 0 & 0 \\ \frac{\mathrm{i}}{\sqrt{2}} & \frac{-\mathrm{i}}{\sqrt{3}} & \frac{-\mathrm{i}}{\sqrt{10}} & \frac{-\sqrt{3}}{\sqrt{170}} & \frac{-\sqrt{5}}{\sqrt{102}} & 0 & 0 & 0 \\ 0 & \frac{-1}{\sqrt{3}} & \frac{\sqrt{2}}{\sqrt{5}} & \frac{-\mathrm{i}\sqrt{6}}{\sqrt{85}} & \frac{-\mathrm{i}\sqrt{10}}{\sqrt{51}} & 0 & 0 & 0 \\ 0 & 0 & \frac{\sqrt{2}}{\sqrt{5}} & \frac{\mathrm{i}3\sqrt{3}}{\sqrt{170}} & \frac{\mathrm{i}\sqrt{15}}{\sqrt{34}} & 0 & 0 & 0 \\ 0 & 0 & 0 & \frac{\sqrt{15}}{\sqrt{34}} & \frac{-3\sqrt{3}}{\sqrt{170}} & \frac{\mathrm{i}\sqrt{2}}{\sqrt{5}} & 0 & 0 \\ 0 & 0 & 0 & \frac{-\sqrt{10}}{\sqrt{51}} & \frac{\sqrt{6}}{\sqrt{85}} & \frac{\mathrm{i}\sqrt{2}}{\sqrt{5}} & \frac{\mathrm{i}}{\sqrt{3}} & 0 \\ 0 & 0 & 0 & \frac{\mathrm{i}\sqrt{5}}{\sqrt{102}} & \frac{-\mathrm{i}\sqrt{3}}{\sqrt{170}} & \frac{1}{\sqrt{10}} & \frac{-1}{\sqrt{3}} & \frac{-1}{\sqrt{2}} \\ 0 & 0 & 0 & \frac{\mathrm{i}\sqrt{5}}{\sqrt{102}} & \frac{-\mathrm{i}\sqrt{3}}{\sqrt{170}} & \frac{1}{\sqrt{10}} & \frac{-1}{\sqrt{3}} & \frac{1}{\sqrt{2}} \end{pmatrix} \tag{9}$$

The unitary matrix in Eq. (9) expresses an optical transformation on a beam-splitter network consisting of seven beam splitters and can be decomposed into $U_D = F_8^\dagger F_7 F_4 F_3^\dagger I_2(-1) I_1(-1) B_{78}^-(1/2) F_8 B_{12}^-(1/2) F_1 B_{67}^-(1/3) F_7 B_{23}^-(1/3) F_2 B_{56}^-(2/5) F_6 B_{34}^-(2/5) F_3 B_{45}^+(25/34)$, where F_k denotes the Fourier transformation of mode k, which corresponds to a 90° rotation in the phase space; $B_{kl}^\pm(T_j)$ stands for the linearly optical transformation on the jth beam-splitter with the transmission of T_j ($j = 1,2,3,\cdots,7$), where $(B_{kl}^\pm)_{kk} = \sqrt{1-T}$, $(B_{kl}^\pm)_{kl} = \sqrt{T}$, $(B_{kl}^\pm)_{lk} = \pm\sqrt{T}$, and $(B_{kl}^\pm)_{ll} = \mp\sqrt{1-T}$, are elements of beam-splitter matrix. $I_k(-1) = \mathrm{e}^{\mathrm{i}\pi}$ corresponds to a 180° rotation of mode k in the phase space. The transmissions of the seven beam splitters are chosen as $T_1 = 25/34$, $T_2 = T_3 = 2/5$, $T_4 = T_5 = 1/3$ and $T_6 = T_7 = 1/2$. The excess noise terms of the nullifiers in the two-diamond shape cluster state are expressed by $\delta_{D_1} = -\frac{1}{\sqrt{2}}\mathrm{e}^{-r}\hat{x}_1^{(0)} + \sqrt{\frac{5}{2}}\mathrm{e}^{-r}\hat{x}_3^{(0)}$, $\delta_{D_2} = \frac{1}{\sqrt{2}}\mathrm{e}^{-r}\hat{x}_1^{(0)} - \sqrt{\frac{5}{2}}\mathrm{e}^{-r}\hat{x}_3^{(0)}$, $\delta_{D_3} = -\sqrt{3}\mathrm{e}^{-r}\hat{p}_2^{(0)}$, $\delta_{D_4} = -\frac{2}{\sqrt{3}}\mathrm{e}^{-r}\hat{p}_2^{(0)} + \sqrt{\frac{2}{5}}\mathrm{e}^{-r}\hat{p}_6^{(0)} + \sqrt{\frac{34}{15}}\mathrm{e}^{-r}\hat{x}_5^{(0)}$, $\delta_{D_5} = \sqrt{\frac{34}{15}}\mathrm{e}^{-r}\hat{p}_4^{(0)} - \sqrt{\frac{2}{5}}\mathrm{e}^{-r}\hat{x}_3^{(0)} + \frac{2}{\sqrt{3}}\mathrm{e}^{-r}\hat{x}_7^{(0)}$, $\delta_{D_6} = \sqrt{3}\mathrm{e}^{-r}\hat{x}_7^{(0)}$, $\delta_{D_7} = \sqrt{\frac{5}{2}}\mathrm{e}^{-r}\hat{p}_6^{(0)} - \frac{1}{\sqrt{2}}\mathrm{e}^{-r}\hat{p}_8^{(0)}$, and $\delta_{D_8} = \sqrt{\frac{5}{2}}\mathrm{e}^{-r}\hat{p}_6^{(0)} + \frac{1}{\sqrt{2}}\mathrm{e}^{-r}\hat{p}_8^{(0)}$, respectively.

2.2 Inseparability criteria for the cluster state

According to the inseparability criteria for CV multipartite entangled states proposed by van Loock and Furusawa [20], we deduce the concrete inseparability conditions for CV eight-partite two-diamond shape cluster state. For any separable quantum state, its total density operator can be written as $\hat{\rho} = \sum_i \eta_i \hat{\rho}_{i,k,\cdots,m} \otimes \hat{\rho}_{i,l,\cdots,n}$ with a distinct pair of "separable modes" (m,n) and the other modes $k \neq l$ [see Eq. (25) in Ref. 20], where η_i represent the mixture of these separable states. For any combinations $\hat{u} = h_1\hat{x}_1 + h_2\hat{x}_2 + \cdots + h_N\hat{x}_N$ and $\hat{v} = g_1\hat{p}_1 + g_2\hat{p}_2 + \cdots + g_N\hat{p}_N$, the inseparability criteria are expressed by [20]

$$V(\hat{u}) + V(\hat{v}) < \frac{1}{2}\Big(\Big| h_m g_m + \sum\nolimits_k h_k g_k \Big| + \Big| h_n g_n + \sum\nolimits_l h_l g_l \Big| \Big) \tag{10}$$

The inseparability criteria for CV eight-partite two-diamond shape cluster state deduced from Eq. (10) are expressed by the following inequalities:

$$V(\hat{p}_{D_1} - \hat{x}_{D_3} - g_{D_1}\hat{x}_{D_4}) + V(\hat{p}_{D_3} - \hat{x}_{D_1} - g_{D_2}\hat{x}_{D_2}) < 1 \tag{11a}$$

$$V(\hat{p}_{D_2} - \hat{x}_{D_3} - g_{D_1}\hat{x}_{D_4}) + V(\hat{p}_{D_3} - \hat{x}_{D_2} - g_{D_2}\hat{x}_{D_1}) < 1 \tag{11b}$$

$$V(\hat{p}_{D_1} - g_{D_3}\hat{x}_{D_3} - \hat{x}_{D_4}) + V(\hat{p}_{D_4} - \hat{x}_{D_1} - g_{D_4}\hat{x}_{D_2} - g_{D_5}\hat{x}_{D_5}) < 1 \tag{11c}$$

$$V(\hat{p}_{D_2} - g_{D_3}\hat{x}_{D_3} - \hat{x}_{D_4}) + V(\hat{p}_{D_4} - g_{D_4}\hat{x}_1 - \hat{x}_{D_2} - g_{D_5}\hat{x}_{D_5}) < 1 \tag{11d}$$

$$V(\hat{p}_{D_4} - g_{D_6}\hat{x}_{D_1} - g_{D_6}\hat{x}_{D_2} - \hat{x}_{D_5}) + V(\hat{p}_{D_5} - \hat{x}_{D_4} - g_{D_6}\hat{x}_{D_7} - g_{D_6}\hat{x}_{D_8}) < 1 \tag{11e}$$

$$V(\hat{p}_{D_5} - g_{D_5}\hat{x}_{D_4} - \hat{x}_{D_7} - g_{D_4}\hat{x}_{D_8}) + V(\hat{p}_{D_7} - \hat{x}_{D_5} - g_{D_3}\hat{x}_{D_6}) < 1 \tag{11f}$$

$$V(\hat{p}_{D_5} - g_{D_5}\hat{x}_{D_4} - g_{D_4}\hat{x}_{D_7} - \hat{x}_{D_8}) + V(\hat{p}_{D_8} - \hat{x}_{D_5} - g_{D_3}\hat{x}_{D_6}) < 1 \tag{11g}$$

$$V(\hat{p}_{D_6} - \hat{x}_{D_7} - g_{D_2}\hat{x}_{D_8}) + V(\hat{p}_{D_7} - g_{D_1}\hat{x}_{D_5} - \hat{x}_{D_6}) < 1 \tag{11h}$$

$$V(\hat{p}_{D_6} - g_{D_2}\hat{x}_{D_7} - \hat{x}_{D_8}) + V(\hat{p}_{D_8} - g_{D_1}\hat{x}_{D_5} - \hat{x}_{D_6}) < 1 \tag{11i}$$

The left-hand sides and right-hand sides of these inequalities are the combination of variances of nullifiers and the boundary, respectively. When all inequalities in Eq. (11) are satisfied, CV eight-partite two-diamond shape cluster entanglement is demonstrated. Calculating the minimal values of the left-hand sides of the inequalities versus the gain factors ($g_{D_1-D_6}$) for the two-diamond shape eight-partite cluster state, we can obtain the optimal gain factors $g_{D_1-D_6}^{opt}$ for achieving the detections of the minimal correlation variances. For the two diamond ($g_{D_1-D_6}^{opt}$) cluster states the optimal gain factors are $g_{D_1} = \frac{15(\mathrm{e}^{4r}-1)}{19+15\mathrm{e}^{4r}}$, $g_{D_2} = \frac{21(\mathrm{e}^{4r}-1)}{13+21\mathrm{e}^{4r}}$, $g_{D_3} = \frac{9(\mathrm{e}^{4r}-1)}{8+9\mathrm{e}^{4r}}$, $g_{D_4} = \frac{9(\mathrm{e}^{8r}-1)}{7+18\mathrm{e}^{4r}+9\mathrm{e}^{8r}}$, $g_{D_5} = \frac{3(3\mathrm{e}^{8r}-2\mathrm{e}^{4r}-1)}{7+18\mathrm{e}^{4r}+9\mathrm{e}^{8r}}$, and $g_{D_6} = \frac{4(\mathrm{e}^{4r}-1)}{13+4\mathrm{e}^{4r}}$, respectively.

The dependence of inseparability criteria of the CV eight-partite two-diamond shape cluster state on the squeezing parameter is shown in Fig. 2. Since the variances of inequalities (11a), (11b), (11h) and (11i) are the same, and that of (11c), (11d), (11f) and (11g) are also the same, we only plot the correlation variances of the inequalities (11a), (11c) and (11e) in Fig. 2(a), (b) and (c), respectively. From Fig. 2(a), (b) and (c), we can see that when the squeezing parameters $r > 0.20$ for Fig. 2(a), $r > 0.28$ for Fig. 2(b), and $r > 0.35$ for Fig. 2(c), the correlation variances (curve 1) are smaller than the boundary for the case of $g = 1$. It means that if taking $g = 1$, a lower limitation for the squeezing parameter is required satisfy these inseparability criteria. However, if taking the optimal gain factor g^{opt} (curve 3), all variances are below the boundary for any value of $r > 0$.

3 The experiment

Figure 1(b) shows the schematic of the experimental set-up for preparing the eight-partite CV two-diamond shape cluster state. The four $\hat{x}$ -squeezed and four $\hat{p}$-squeezed states are produced by four nondegenerate optical parametric amplifiers (NOPAs) pumped by a common laser source, which is a CW intracavity frequency-doubled and frequency-stabilized Nd:YAP/LBO(Nd-doped $YAlO_3$ perorskite/lithium triborate) with both outputs of the fundamental and the second-harmonic waves [24]. The output fundamental wave at 1080 nm wavelength is used for the injected signals of NOPAs and the local oscillators of the balanced homodyne detectors (BHDs), which are applied to measure the quantum fluctuations of the quadrature-amplitude and the quadrature-phase of the output optical modes [15]. The second-harmonic wave at 540 nm wavelength serves as the pump field of the four NOPAs, in which through an intracavity frequency-down-conversion process a pair of signal and idler modes with the identical frequency at 1080 nm and the orthogonal polarizations are generated [25, 26]. Each of the NOPAs consists of an α-cut type-II KTP crystal and a concave mirror [26]. The front face of the KTP was coated to be used for the input coupler and the concave mirror serves as the output coupler of the squeezed states, which is mounted on a piezo-electric transducer for locking actively the cavity length of NOPA on resonance with the injected signal at 1080 nm. The transmissions of the input coupler at 540 nm and 1080 nm are 99.8% and 0.04%, respectively. The transmissions of the output coupler at 540 nm and 1080 nm are 0.5% and 5.2%, respectively. The finesses of the NOPA for 540 nm and 1080 nm are 3 and 117, respectively. In our experiment, the four NOPAs are operated at the parametric deamplification situation, i.e., the phase difference between the pump fields and the injected signal is $(2n + 1)\pi$ (n is an integer). Under this condition, the coupled modes at $+45°$ and $-45°$ polarization directions are the quadrature-amplitude and the quadrature-phase squeezed states, respectively [15, 27]. When the transmissions of the seven beam splitters are chosen as $T_1 = 25/34$, $T_2 = T_3 = 2/5$, $T_4 = T_5 = 1/3$, $T_6 = T_7 = 1/2$, the eight output optical modes $\hat{b_j}$ ($j = 1, 2, \cdots, 8$) are in a eight-partite CV two-diamond shape cluster state. The quadrature-amplitude and quadrature-phase of each $\hat{b_j}$ are measured by eight BHDs, respectively. The nullifiers of the eight output modes depend on the squeezing parameters of the resource squeezed states. For our experimental system all four NOPAs have the identical configuration and are operated under the same conditions. So, the eight initial squeezed states own the same squeezed parameter r.

The experimentally measured initial squeezing degrees of the output fields from the four NOPAs were 4.30±0.07 dB below the QNL which corresponded to the squeezing parameter $r = 0.50 \pm 0.02$. For our system, the total transmission efficiency of squeezed beams were about 87% and the detection efficiency is about 90%, which led to the efficient squeezing parameter $r_e = 0.30$ which was smaller than the initially measured squeezing. During the measurements the pump power of NOPAs at 540 nm

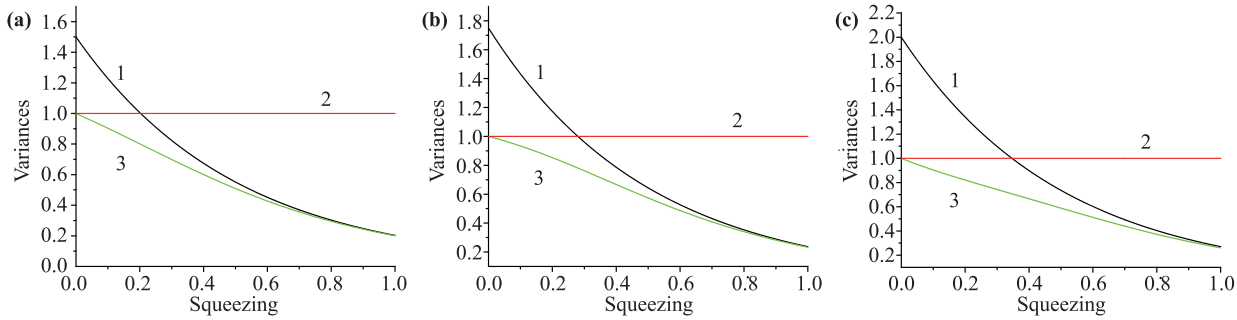

Fig. 2 The dependence of eight-partite two-diamond shape cluster state to squeezing parameter, **(a)**, **(b)** and **(c)** are corresponding to inequalities (11a), (11c), and (11e), respectively. Lines 1 and 3 are left-hand sides of inequalities with unit gain and optimal gain, respectively, line 2 is the boundary at the right-hand side of inequalities.

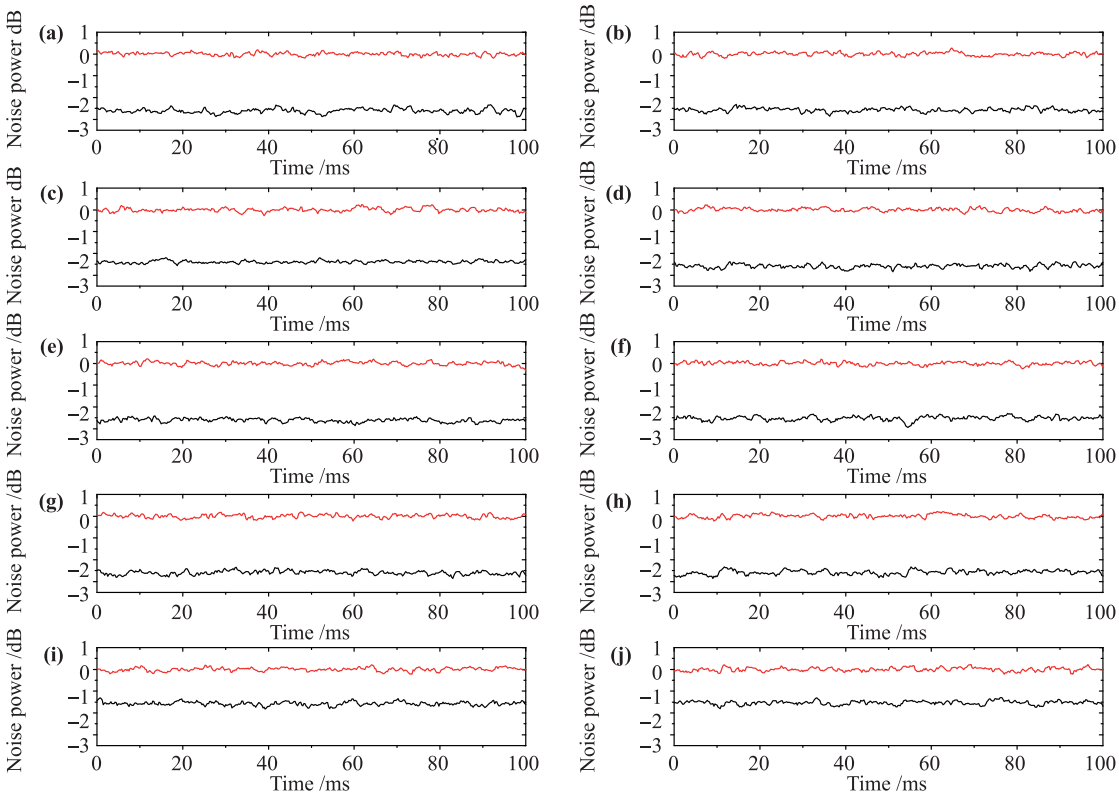

Fig. 3 The measured noise powers of the eight-partite two-diamond shape cluster state. The upper and lower lines in all graphs are shot noise level and correlation variances of nullifiers, respectively. **(a)**–**(j)** are noise powers of $V(\hat{p}_{D_1}-\hat{x}_{D_3}-\hat{x}_{D_4})$, $V(\hat{p}_{D_2}-\hat{x}_{D_3}-\hat{x}_{D_4})$, $V(\hat{p}_{D_3}-\hat{x}_{D_1}-\hat{x}_{D_2})$, $V(\hat{p}_{D_4}-\hat{x}_{D_1}-\hat{x}_{D_2}-\hat{x}_{D_5})$, $V(\hat{p}_{D_5}-\hat{x}_{D_4}-\hat{x}_{D_7}-\hat{x}_{D8})$, $V(\hat{p}_{D_6}-\hat{x}_{D_7}-\hat{x}_{D_8})$, $V(\hat{p}_{D_7}-\hat{x}_{D_5}-\hat{x}_{D_6})$, $V(\hat{p}_{D_8}-\hat{x}_{D_5}-\hat{x}_{D_6})$, $V(\hat{p}_{D_4}-g_{D_6}\hat{x}_{D_1}-g_{D_6}\hat{x}_{D_2}-\hat{x}_{D_5})$, $V(\hat{p}_{D_5}-\hat{x}_{D_4}-g_{D_6}\hat{x}_{D_7}-g_{D_6}\hat{x}_{D_8})$, respectively. The measurement frequency is 2 MHz, resolution bandwidth is 30 kHz, video bandwidth is 100 Hz, $g_{D_1-D_5}=1$ and $g_{D_6}=g_{D_6}^{opt}=0.60\pm0.02$.

wavelength was kept at $\sim$ 180 mW, which was below the oscillation threshold of 240 mW of the NOPAs, and the intensity of the injected signal at 1080 nm was 10 mW. The phase difference on each beam-splitters were locked according to the requirements. The light intensity of the local oscillator in all BHDs was set to around 5 mW. The measured QNL was about 20 dB above the electronics noise level, which guaranteed that the results of the homodyne detections were almost not affected by electronic noises. The correlation variances measured experimentally are shown in Fig. 3 for the two-diamond shape cluster state. They are $V(\hat{p}_{D_1}-\hat{x}_{D_3}-\hat{x}_{D_4})=-2.61\pm0.10$ dB, $V(\hat{p}_{D_2}-\hat{x}_{D_3}-\hat{x}_{D_4})=-2.57\pm0.09$ dB, $V(\hat{p}_{D_3}-\hat{x}_{D_1}-\hat{x}_{D_2})=-2.39\pm0.06$ dB, $V(\hat{p}_{D_4}-\hat{x}_{D_1}-\hat{x}_{D_2}-\hat{x}_{D_5})=-2.58\pm0.09$ dB, $V(\hat{p}_{D_5}-\hat{x}_{D_4}-\hat{x}_{D_7}-\hat{x}_{D_8})=-2.61\pm0.09$ dB, $V(\hat{p}_{D_6}-\hat{x}_{D_7}-\hat{x}_{D_8})=-2.52\pm0.10$ dB, $V(\hat{p}_{D_7}-\hat{x}_{D_5}-\hat{x}_{D_6})=-2.59\pm0.09$ dB, $V(\hat{p}_{D_8}-\hat{x}_{D_5}-\hat{x}_{D_6})=-2.58\pm0.10$ dB, $V(\hat{p}_{D_4}-g_{D_6}\hat{x}_{D_1}-g_{D_6}\hat{x}_{D_2}-\hat{x}_{D_5})=-1.57\pm0.09$ dB, and $V(\hat{p}_{D_5}-\hat{x}_{D_4}-g_{D_6}\hat{x}_{D_7}-g_{D_6}\hat{x}_{D_8})=-1.53\pm0.09$ dB. From these measured results we calculated the combinations of the correlation variances in the left-hand sides of the inequalities (11a)–(11i), which are 0.84 ± 0.02, 0.85 ± 0.02, 0.96 ± 0.02, 0.97 ± 0.02, 0.95 ± 0.02, 0.96 ± 0.02, 0.96 ± 0.02, 0.83 ± 0.02, 0.83 ± 0.02, respectively. All these values are smaller than the boundary of 1. It means that the prepared CV cluster state satisfies the inseparability criteria for verifying eight-partite CV entanglement.

4 Conclusion

In the conclusion, we have experimentally prepared spatially separated eight-partite two-diamond shape CV cluster entangled state by using eight quadrature squeezed states of light and a specifically designed optical beam-splitter network. The multipartite entangled states are the essential resources to construct a variety of CVQI networks. So far, the single-mode squeezed states over 12.7 dB [28] and the two-mode squeezed states over 8.1 dB [29] have been experimentally generated, respectively. Therefore the CV cluster state with more space-separable qumodes and higher entanglement are able to be realized. The complexity and versatility of CV multipartite entanglement for photonic qumodes not only offer richly potential applications in QC and

QI, but also provide the basic and handleable quantum states for studying the important and attractive quantum phenomena.

Acknowledgements This research was supported by the National Basic Research Program of China (Grant No. 2010CB923103) and the National Natural Science Foundation of China (Grant Nos. 11174188 and 61121064) and Shanxi Scholarship Council of China (Grant No. 2012-010).

References

1. M. A. Nielsen and I. L. Chuang, Quantum Computation and Quantum Information, Cambridge: Cambridge University Press, 2000
2. S. L. Braunstein and P. van Loock, Rev. Mod. Phys., 2005, 77(2): 513
3. R. Raussendorf and H. J. Briegel, Phys. Rev. Lett., 2001, 86(22): 5188
4. N. C. Menicucci, P. van Loock, M. Gu, C. Weedbrook, T. C. Ralph, and M. A. Nielsen, Phys. Rev. Lett., 2006, 97(11): 110501
5. P. Walther, K. J. Resch, T. Rudolph, E. Schenck, H. Weinfurter, V. Vedral, M. Aspelmeyer, and A. Zeilinger, Nature, 2005, 434(7030): 169
6. K. Chen, C. M. Li, Q. Zhang, Y. A. Chen, A. Goebel, S. Chen, A. Mair, and J. W. Pan, Phys. Rev. Lett., 2007, 99(12): 120503
7. W. Gao, P. Xu, X. Yao, O. Gühne, A. Cabello, C. Y. Lu, C. Z. Peng, Z. B. Chen, and J. W. Pan, Phys. Rev. Lett., 2010, 104(2): 020501
8. P. van Loock, J. Opt. Soc. Am. B, 2007, 24: 340
9. A. Tan, C. Xie, and K. Peng, Phys. Rev. A, 2009, 79(4): 042338
10. M. Gu, C. Weedbrook, N. C. Menicucci, T. C. Ralph, and P. van Loock, Phys. Rev. A, 2009, 79(6): 062318
11. Y. Miwa, J. I. Yoshikawa, P. van Loock, and A. Furusawa, Phys. Rev. A, 2009, 80(5): 050303(R)
12. Y. Wang, X. Su, H. Shen, A. Tan, C. Xie, and K. Peng, Phys. Rev. A, 2010, 81(2): 022311
13. R. Ukai, N. Iwata, Y. Shimokawa, S. C. Armstrong, A. Politi, J. Yoshikawa, P. van Loock, and A. Furusawa, Phys. Rev. Lett., 2011, 106(24): 240504
14. R. Ukai, S. Yokoyama, J. I. Yoshikawa, P. van Loock, and A. Furusawa, Phys. Rev. Lett., 2011, 107(25): 250501
15. X. Su, A. Tan, X. Jia, J. Zhang, C. Xie, and K. Peng, Phys. Rev. Lett., 2007, 98(7): 070502
16. M. Yukawa, R. Ukai, P. van Loock, and A. Furusawa, Phys. Rev. A, 2008, 78(1): 012301
17. A. Tan, Y. Wang, X. Jin, X. Su, X. Jia, J. Zhang, C. Xie, and K. Peng, Phys. Rev. A, 2008, 78(1): 013828
18. M. Pysher, Y. Miwa, R. Shahrokhshahi, R. Bloomer, and O. Pfister, Phys. Rev. Lett., 2011, 107(3): 030505
19. X. Su, Y. Zhao, S. Hao, X. Jia, C. Xie, and K. Peng, Opt. Lett., 2012, 37(24): 5178
20. P. van Loock and A. Furusawa, Phys. Rev. A, 2003, 67(5): 052315
21. J. Zhang and S. L. Braunstein, Phys. Rev. A, 2006, 73(3): 032318
22. P. van Loock, C. Weedbrook, and M. Gu, Phys. Rev. A, 2007, 76(3): 032321
23. N. C. Menicucci, S. T. Flammia, and P. van Loock, Phys. Rev. A, 2011, 83(4): 042335
24. Y. Wang, Y. Zheng, C. Xie, and K. Peng, IEEE J. Quantum Electron., 2011, 47(7): 1006
25. X. Li, Q. Pan, J. Jing, J. Zhang, C. Xie, and K. Peng, Phys. Rev. Lett., 2002, 88(4): 047904
26. Y. Wang, H. Shen, X. Jin, X. Su, C. Xie, and K. Peng, Opt. Express, 2010, 18(6): 6149
27. Y. Zhang, H. Wang, X. Li, J. Jing, C. Xie, and K. Peng, Phys. Rev. A, 2000, 62(2): 023813
28. T. Eberle, S. Steinlechner, J. Bauchrowitz, V. Händchen, H. Vahlbruch, M. Mehmet, H. Müller-Ebhardt, and R. Schnabel, Phys. Rev. Lett., 2010, 104(25): 251102
29. Z. Yan, X. Jia, X. Su, Z. Duan, C. Xie, and K. Peng, Phys. Rev. A, 2012, 85(4): 040305(R)